Piezoelectric Vibrations Energy Harvesters Power Optimization Using the Finite Element Method

A.M. Matos∗[1], J.M. Guedes∗[2], K.P. Jayachandran, H.C. Rodrigues

IDMEC, IST, Department of Mechanical Engineering, Technical University of Lisbon, Av. Rovisco Pais, 1049-001 Lisbon, Portugal

∗[1]ago.matoz@gmail.com ; ∗[2]jmguedes@tecnico.ulisboa.pt

October, 2014

Abstract: This paper presents a computational model using the finite element (FE) method to simulate piezoelectric vibrations energy harvesters for power optimization in the context of small size applications. A version of the simulated annealing algorithm is used to optimize power. Four common configurations, viz; longitudinal generator, transverse generator, unimorph and bimorph are considered. The electrical machine linked to the harvester is represented by a resistance. In the first part of the study, the FE model is validated. In the second part, the harvested power is optimized varying material orientation and changing piezoelectric material between $BaTiO_3$ and PZT-5H in non-resonance for different 1Hz loadings. It is observed that the best material orientation & best material can change with the loading type and the results are discussed. In the third part, the material orientation optimization is performed near resonance frequency for unimorph and bimorph configurations. The need to include material's hysteretic damping is demonstrated. Moreover, the optimal orientation near resonance excitation can be different from those obtained for 1 Hz. Results are shown and discussed. Next the power sensibility to resistance is presented for resonance maximum power orientations; results are discussed. Finally unimorph harvested power is optimized for a collection of frequencies near resonance; results are discussed.

1. Introduction

The technological development that happened along years with computers, mobile phones and others showing increased power efficiency over time encourage scientists and engineers to think about energy harvesters powering low power consumption devices. Nowadays with the human impact on day to day life there are two sources of energy which can be harvested, i.e., natural energy and human technology. The natural energy sources are the wind, waves, solar, human movements and so on. The human technology energy sources are engines, industrial machines movement, wash machines, etc. Past works [1 to 2] have shown power harvesting using piezoelectric materials as possible using these sources. However they also show that a single piezoelectric harvester produces low power. For example a piezofiber composite plate of 2.2 cm^3 produces 120 mW. This creates the need to increase the power which harvesters can produce.

This paper is focused in the conversion of vibration energy into electrical energy using piezoelectric materials. All types of energy sources are considered as long they cause vibrations. Various works [1 to 7] have been reported studying piezoelectric materials as vibration energy harvesters. Some important conclusions from these references to this work are presented next. Past works showed lead zirconate titanate (PZT) to be one of the most efficient materials for power harvesting. However PZTs have a brittle nature and a low tensile strength causing a limitation to the stress the material can take. For example, the PZT-5H [8] has a tensile strength of 75.84 MPa. Past works showed that piezoelectric harvesters can work in -33 mode or axial mode and -13 mode or bending mode. The $-ij$ mode means that a time variable strain occurs in direction i causing an electrical field in j direction. In the work [7] to identify properly day by day vibrations which can be used by harvesters it is measured acceleration vs frequency for various ambient vibrations sources. It is found first acceleration peaks occur for frequencies in the range 1 to 200 Hz plus the higher frequency peaks have lower accelerations. In parallel to these experiments a theoretical work [6] shows that when a circuit is connected to the piezoelectric material to harvest mechanical vibrations energy the physical solution of the piezoelectric material (displacements, electrical field, etc) is mathematically coupled with the physical solution of the connected circuit (current, potential difference, etc). In other words, a coupled circuit & piezoelectric material system of equations results. Various works have proposed analytical solutions [3 to 6 & 9 to 17] and FE method solutions [3 to 4 & 18 to 24] to this problem. The works [3 to 4], [21], [23 to 24] present FE analysis results in good agreement with the experimental ones showing the finite element method as a tool suitable to analyze piezoelectric energy harvesters. When modelling piezoelectric materials using the FE method the piezoelectric material properties are assumed constant. However the properties can change with electrical field and others as presented in [25]. This is one limitation of the current finite element methods. Piezoelectric materials have hysteretic damping associated with dielectric, mechanical and piezoelectric losses. Near resonance the mechanical losses are the most significant of the three [26]. This hysteretic damping can be modelled using the FE method considering a constant damping ratio [19].

In parallel to the previous studies the homogenization theory has been used as a tool to tailor piezoelectric materials and represent polycrystalline piezoelectric materials [27 to 31]. One of the methods used consists in calculating the equivalent mechanical properties of a material whose microstructure repeats infinitely, i.e., the microstructure is periodic and the size of the periodic microstructure is much smaller than the material one. This opens the possibility and the interest of having composites microstructures with different materials orientations, microstructure with holes and so on.

This paper is divided in three parts. In the first part the linear piezoelectric constitutive equations are presented and its validity is discussed. The problem governing equations are presented and the FE models are validated. In the second part the harvested power is optimized varying material orientation for different loadings using the FE models faraway resonance. The third part introduces the damping ratio to model hysteretic damping. It is optimized the harvested power for modal frequencies varying material orientation. Next the power sensibility to resistance value is observed for maximum resonance power orientations. Finally the unimorph power is optimized for a collection of frequencies.

2. Piezoelectric Problem, Harvesters Configurations, Material Properties & FE Model Validation

In this section the linear piezoelectric equations are revisited and its applicability is discussed. The overall harvesters physics is presented. A FE model is developed and validated using theoretical results.

2.1. Linear Piezoelectric Constitutive Equations, Electrodes & Conductors Resistivity

Considering the displacement gradient $u_{i,M}$ and electrical potential $\phi_{,K}$ being infinitesimals, i. e., $|u_{i,K}| \ll 1$ & $|\phi_{,K}| \ll 1$ the linear piezoelectric material constitutive equations are obtained [32]:

$$\{S\} = [S^E]\{T\} + [d]^t\{E_k\} \quad (1.1)$$
$$\{D\} = [d]\{T\} + [\varepsilon^T]\{E_k\} \quad (1.2)$$

In the equations 1 $\{S\}$ is the strain vector, $[S^E]$ is the compliance measured in constant electrical field, $\{T\}$ is the stress vector, $[\varepsilon^T]$ is the dielectric matrix measured in constant stress, $\{E_k\} = \phi_{,k}$ is the electrical field, $\{D\}$ is the electrical displacement and $[d]$ is the electric polarization generated in the material per unit mechanical stress applied to it. Each d_{ij} element of matrix $[d]$ is the induced polarization in direction i per unit stress applied in direction j (note $[d]$ is a 3x6 matrix). Note in these equations the superscript t outside a matrix means it is its transpose matrix. Observing equation 1 it is noted that an applied electrical field or stress causes material deformation and electrical displacement.

In piezoelectric vibration energy harvesters typically electrodes are used to link the piezoelectric material to the circuit. Each electrode has a constant electrical potential on a surface S_ϕ. The total free electrical charge crossing S_ϕ is given by expression 2. The change of free electrical charge over time results in a current going out of the electrode which is given by expression 3.

$$Q_e = \int_{S_\phi} -n_i D_i dS \quad (2)$$
$$I = -\dot{Q}_e \quad (3)$$

In some configurations of piezoelectric energy harvesters electrical conductor materials are used as substrate. The conductivity can be modeled using the FE method as a circuit connecting electrodes or others with an equivalent resistance using:

$$R_{eq} = \frac{r_e l}{A} \quad (4)$$

where r_e is the material resistivity, A is the cross section area and l is the length of the conductor perpendicular to area A.

2.2. Linear Piezoelectric Constitutive Equations for Non Infinitesimal Electrical Fields

In other works [3,12 & 19] for some configurations high electrical fields have been observed, i. e., $|\phi_{,K}|$ not $\ll 1$. This creates the need to understand for which conditions the constitutive equations are still linear. The problem of determining the piezoelectric constitutive equations [32] is to solve equations 5. The total energy density is given by K where strain and electrical field terms higher than order 2 are not presented plus products of them being higher than order 2. In expression 5.1 $C_{2_{ijkl}}$ is second order elastic tensor (constant), S_{mn} is the strain tensor, e_{ijk} piezoelectric tensor (constant), $\Upsilon_{2_{\mathrm{ij}}}$ the electric susceptibility (constant), ε_0 is the vacuum permittivity and E_h the electric field. In expression 5.2 T^S_{KL} is the symmetric stress tensor and T^M_{KL} is the symmetric Maxwell stress tensor. D_K is the electrical displacement in expression 5.3. The upper cases letters indicate that the quantities are written in reference coordinates and lower case letters indicate that quantities are written in present coordinates.

$$K = \frac{1}{2}C_{2_{ABCD}}S_{AB}S_{CD} - e_{ABC}E_A S_{BC} - \frac{1}{2}\Upsilon_{2_{\mathrm{AB}}}E_A E_B + high\ order\ terms - \frac{1}{2}\varepsilon_0 J E_k E_k \quad (5.1)$$

$$\frac{\partial K}{\partial S_{KL}} = T^S_{KL} + T^M_{KL} = total\ stress\ tensor \quad (5.2)$$

$$\frac{\partial K}{\partial E_K} = -D_K \quad (5.3)$$

Supposing $|u_{i,K}| \ll 1$ it results [32]:

$$E_K \cong E_k\ ;\ S_{kl} \cong \frac{1}{2}(u_{l,k} + u_{k,l});\ D_K \cong D_k\ ;\ P_K \cong P_k$$
$$T^S_{KL} \cong T^S_{kl}\ ;\ T^M_{KL} \cong T^M_{kl}\ etc \quad (6)$$

Using 6 and rewriting equations of material in terms of present coordinates (lower case letters) results in:

$$\tau_{ij} = \sigma_{ij} + P_i E_j + \varepsilon_0\left(E_i E_j - \frac{1}{2}E_k E_k \delta_{ij}\right) \quad (7)$$
$$\sigma^S_{ij} = \sigma_{ij} + P_i E_j \quad (8)$$

where σ_{ij} is the Cauchy stress tensor, τ_{ij} is the total stress tensor, σ^S_{ij} symmetric stress tensor and P_i is polarization. Observing equations 5 and equation 7 it is concluded that linear piezoelectric constitutive equations are still valid in a presence of a not infinitesimal electrical field if:

a) high order terms in K are not significant
b) $\sigma_{ij} \gg P_i E_j + \varepsilon_0\left(E_i E_j - \frac{1}{2}E_k E_k \delta_{ij}\right)$

2.3. The Piezoelectric Harvesters Governing Equations & Boundary Conditions

A piezoelectric harvester can be modelled using the FE method or other numerical method. The differential equations to solve are the same. Typically it is solved the system of equations (9). Going from up to down it is identified the motion equation, charge equation, stress and displacement relations, electrical field and potential relations, electric machine equations and finally the constitutive equations.

$$\begin{cases} T_{ji,j} = \rho\ddot{u}_i \\ D_{i,i} = 0 \\ S_{ij} = \dfrac{u_{i,j} + u_{j,i}}{2}\ ;\ E_i = -\phi_{,i} \\ \text{Electric machine equations, for a resistor } V = RI \\ \text{Constitutive equations} \end{cases} \quad (9)$$

These equations are solved in a piezoelectric body considering the boundary conditions as illustrated in figure 1. In this figure it is observed imposed electrical potential $\phi = \bar{\phi}\ on\ S_\phi$ (electrodes yellow surfaces) which are connected somehow to a green electric machine, zero electrical flux $D_j n_j = 0\ on\ S_D$ (not electrode surface), specified displacements $u_i = \overline{u_i}\ on\ S_u$ and specified stresses $T_{ij}n_i = \overline{t_j}\ on\ S_T$. Note the piezoelectric material surface $S = S_\phi \cup S_D = S_u \cup S_T$.

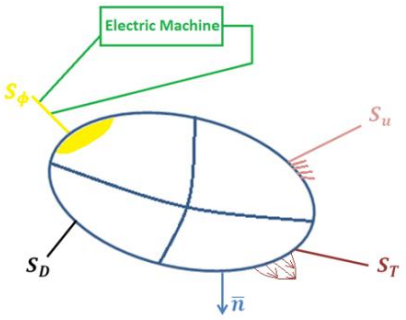

Figure 1 – Piezoelectric body and boundary conditions

2.4. Power Harvested by an Electrical Machine

In piezoelectric vibrations energy harvesters typically the source of energy is free, i.e., it doesn't cost anything. With this in mind the quantity which is desired to measure/calculate is the electrical machine harvested power. This power is given by expression 10 in the complex domain, where I is the current going through the electric machine and V is the potential difference or voltage the electric machine is subjected. The over bar means I and V are represented in the complex domain plus the asterisk in I means it is the complex conjugate of $\bar{I}$. The quantity to be measured/calculated is the nominal electrical power of the electric machine, i. e., the apparent power which is given by 11. The electric machine in this paper is represented by a resistor (for example: a heater) and the apparent power is given by expression 12.

$$\bar{P} = \frac{1}{2}\bar{V}\bar{I}^* \quad (10)$$

$$P_a = |\bar{P}| \quad (11)$$

$$P_a = \frac{1}{2}R|\bar{I}|^2 \quad (12)$$

2.5. Piezoelectric Harvesters Configurations & Circuit Connections

There are many piezoelectric vibration energy harvesters configurations [33]. This work is focused in four typical configurations. These ones are the longitudinal generator, transverse generator, unimorph and bimorph. Each configuration is presented in figure 2. In these figures yellow surfaces represent electrodes. Each electrode surface has an electric potential V_i. These electrodes typically are connected to a green electrical machine. The bimorph configuration has no electric connections since its connections will be explained further. The piezoelectric material is represented as light blue and the substrate as dark blue which is not a piezoelectric material for all configurations. The piezoelectric material polarization or z-direction is represented as an orange arrow with a P by its side. Each harvester configuration has a specific load (represented by red and blue arrows). This load is harmonic being the red arrow one direction of the loading and the blue one the opposite direction. For the longitudinal and transverse generator a harmonic pressure is applied on top and bottom surfaces. For the unimorph and bimorph a harmonic tip moment in a cantilevered beam is applied. Variants of these loadings and boundary conditions can be also applied. The brown variables represent configurations labels for geometrical dimensions.

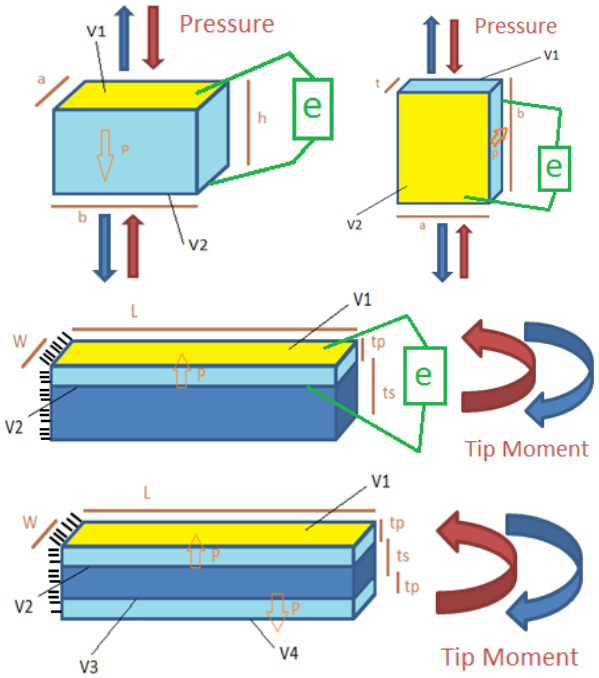

Figure 2 – Piezoelectric harvesters a) longitudinal generator, b) transverse generator, c) unimorph & d) bimorph

There are two typical forms of connecting two piezoelectric harvesters with circuits, i.e., in parallel or in series. These are illustrated in figure 3 where the top and bottom layers are piezoelectric materials with the same dimensions working faraway resonance. Yellow lines indicate electrodes areas. The green resistance is the electrical machine and dark brown resistances are conductors or electrical wires. Piezoelectric materials polarization or z-direction is represented as an orange arrow. The red arrows indicate that the piezoelectric materials are loaded harmonically so that when the top piezoelectric layer is in compression the bottom one is in traction and vice-versa (a cantilevered bimorph loaded by a tip bending moment for example). In series connection the current flows from top to bottom, next to the resistance and back to bottom forming a cycle. In parallel connection the two layers polarization direction is the same causing the current to flow from top and bottom piezoelectric material layers to the electric machine going next to the piezoelectric layers forming a cycle. Since the two piezoelectric layers generate electrical current the electrical machine current will be the double of bimorph series.

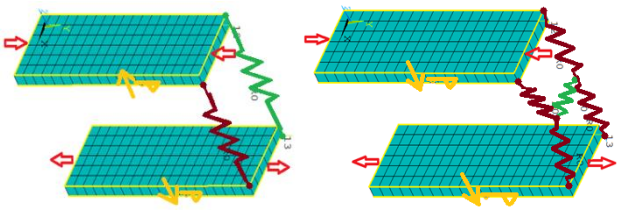

Figure 3 – Harvesters connections in a) series and b) parallel

2.6. Material Properties & Orientation

In this work two piezoelectric materials are considered: $BaTiO_3$ and PZT-5H which are transversely isotropic. The material properties are given in tables 1 to 3 in the IEEE format, i.e., the order used for the piezoelectric matrices is [1,2,3,23,13,12]. These properties are from [34 and 35]. The

PZT-5H and $BaTiO_3$ densities are respectively 7500 and 6020 Kg/m^3.

S^E in $\times\ 10^{-12}\ (m^2/N)$	S_{11}^E	S_{12}^E	S_{13}^E	S_{33}^E	S_{44}^E	S_{66}^E
PZT-5H	16.5	-4.78	-8.45	20.7	43.5	42.6
$BaTiO_3$	7.38	-1.39	-4.41	13.1	16.4	7.46

Table 1 – Piezoelectric materials compliance properties

d *in* $\times\ 10^{-12}\ (C/N)$	d_{31}	d_{33}	d_{15}
PZT-5H	-274	593	741
$BaTiO_3$	-33.72	93.95	560.7

Table 2 – Piezoelectric materials coupling matrix properties

ε^T *in* $\times\ 8.85 \times\ 10^{-12}\ (F/m)$	ε_{11}	ε_{33}
PZT-5H	3130	3400
$BaTiO_3$	2200	56

Table 3 – Piezoelectric materials dielectric coefficients

Since in some configurations a substrate is present, it is still needed to consider a material for it. It is chosen an isotropic brass as substrate. This brass [36 to 37] has a 97 (GPa) Young modulus, Poisson ratio 0.31, density 8490 (Kg/m^3) and a resistivity of $7.1 \times 10^{-8}\ (ohm\ m)$ which is very low revealing the brass conductive nature. The brass has zero dielectric and coupling matrix properties.

The piezoelectric properties can change varying the material orientation since the piezoelectric materials are transversely isotropic. This can cause a change in the harvested power. To characterize the material orientation in this work the Euler angles [38] (ϕ, θ, ψ) are used relative to a right-handed Cartesian coordinate system. This means the material is rotated sequentially ϕ degrees around Z-axis, next θ degrees around new X-axis and finally ψ degrees around new Z-axis. The associated rotation matrix $[a]$ is presented in expressions 13 where ";" separates columns. In this work it is considered Euler angles between -180 to 180 degrees. Each Euler angle can assume only values going with a step of 5 degrees from -180, i. e., -180,-175,-170,-165,…,170,175,180.

$$a_{1j} = [\cos\psi\cos\phi - \cos\theta\sin\phi\sin\psi\,;\cos\psi\sin\phi + \cos\theta\cos\phi\sin\psi\,;\sin\psi\sin\theta] \quad (13.1)$$

$$a_{2j} = [-\sin\psi\cos\phi - \cos\theta\sin\phi\cos\psi\,;-\sin\psi\sin\phi + \cos\theta\cos\phi\cos\psi\ ;\ \cos\psi\sin\theta] \quad (13.2)$$

$$a_{3j} = [\sin\theta\sin\phi\ ;-\sin\theta\cos\phi\,;\ \cos\theta] \quad (13.3)$$

2.7. Out of Resonance Linear Piezoelectric Constitutive Equations Approximation & Power Results

Consider the piezoelectric harvesters of figure 2 with a loading faraway resonance. Supposing the order of magnitude of stresses being $Or[\{T\}] = 1\ MPa$, properties given by section 2.6 and noting $|\phi_{,K}| \ll 1$ the following order of magnitudes results:

$$Or\left[[S^E]\{T\}\right] = 1\times10^{-5};\ Or[[d]^T\{E_k\}] \le 1\times10^{-10}$$
$$Or\left[[d]\{T\}\right] = 1\times10^{-4}\ ;\ \ Or\left[[\varepsilon^T]\{E_k\}\right] \le 1\times10^{-9}$$

This means equations 1 can be approximated with good accuracy by equations 14 which are uncoupled.

$$\{S\} = [S^E]\{T\} \quad (14.1)$$

$$\{D\} = [d]\{T\} \quad (14.2)$$

Now consider that the electrical field is not much smaller than 1. In these conditions the equations 14 are still valid provided that $Or[\{E_k\}] \le 1e4$. This means that if the stress gets one order of magnitude higher, the maximum $Or[\{E_k\}]$ for equations 14 to be valid gets 1 order of magnitude higher too.

Based in the previous approximation power harvested analytical expressions for figure 2 configurations can be obtained faraway resonance using classical mechanics of materials theory [39]. Remember from section 2.4 that the electrical machine is a resistance. Next the electrical current expressions for the different configurations are presented with specific loadings allowing the harvested power to be calculated using equation 12. In the next expressions A refers an electrode area and ω is the applied harmonic load frequency in (rad/s).

A) Longitudinal generator – consider an harmonic pressure σ_{lp} applied on top and bottom surfaces in figure 2.a). Using equations 2 and 3 with 14 it is obtained 15. A more general approach can be found in [6].

$$|I| = |\omega d(3,3)\sigma_{lp}A| \quad (15)$$

B) Transverse generator – consider an harmonic pressure σ_{tp} applied on top and bottom surfaces in figure 2.b) Using equations 2 and 3 with 14 it is obtained:

$$|I| = |\omega d(3,2)\sigma_{tp}A| \quad (16)$$

C) Unimorph – consider a harmonic tip bending moment M is applied around the neutral axis in figure 2.c). Then the average axial stress [37] that the piezoelectric layer is subjected is given by expression 17. In this expression j_0 is the distance of the beginning of the piezoelectric material to the neutral axis, I_n is the transformed section moment of inertia and n is the ratio between piezoelectric and substrate axial elasticity values.

$$\overline{\sigma_{ap}} = \frac{n\left|M\left(2j_0 + t_p\right)\right|}{2I_n} \quad (17)$$

Now using 2 and 3 with 14 and 17 it results:

$$|I| = |\omega d(3,2)\overline{\sigma_{ap}}A| \quad (18)$$

A more general bending study can be seen in [13].
D) Bimorph – here the load is the same as for the unimorph. Expressions 17 and 18 can still be used but now the piezoelectric material layer thickness t_p is different and the transformed section is other one. It is needed to take in account if the harvester is connected in series or in parallel.

2.8. General Finite Element Modelling

To model the harvesters using the finite element method it is decided to use ANSYS version 13 Software. The different materials are modelled using SOLID226 linear piezoelectric 20 nodes element. Element SOLID226 has 4 degrees of freedom (DOF) per node, i.e., three translations and a voltage DOF. The electrodes are modelled coupling the voltage DOF on the nodes of the respective surface. To model conductor resistivity or the resistance the element CIRCU94 is used. All the previous elements provide solution for vibration harmonic analysis which is the analysis used in this work.

2.9. Geometry, Loadings and Boundary Conditions & Finite Element Mesh

Defined how the model is created using the finite element method it is necessary to specify the geometry of the different configurations. This is presented in tables 4 and 5. Note in table 5 it is also presented the value of the substrate equivalent resistance.

Configuration	*a(cm)*	*b(cm)*	*t(cm)*	*h(cm)*
Longitudinal Generator	0.387	0.387	---	0.025
Transverse Generator	0.387	0.387	0.025	---

Table 4 – Longitudinal and transverse generators dimensions

Configuration	*L (cm)*	*W(cm)*	*tp(cm)*	*ts(cm)*	R_{eq} *(ohm)*
Unimorph	1	0.15	0.025	0.075	–
Bimorph	1	0.15	0.0125	0.075	3.55e-6

Table 5 – Unimorph and bimorph harvesters dimensions

The next step is to specify the loadings and boundary conditions for the different configurations thinking in terms of geometry. For the longitudinal and transverse generators top and bottom surfaces pressures of 10 MPa harmonic 1 Hz (this load case is labelled P) are applied. For the unimorph and bimorph the beam root has all the displacements equal to zero. In these last two configurations the loading condition is a tip bending moment of 0.00254 (Nm) harmonic 1 Hz (this load case is labelled B) .This is done applying a force of 1.2685 (N) in each one of the four cantilever tip corners. Note that at the top corners the force will point from root to tip and in the bottom corners the force will point from tip to root or vice-versa. For the four configurations an electrode connected to the ground is specified, i. e., $V_2 = 0$.

After the loading and boundary conditions are defined the required mesh is obtained for converged electrical machine power results. The meshes are presented in figure 4. The blue portions are piezoelectric material and the rocky ones are substrate or brass material.

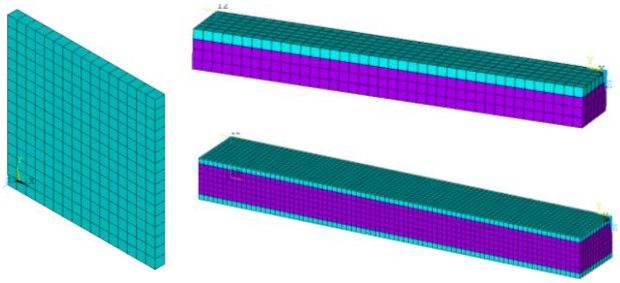

Figure 4 – FE model meshes a) longitudinal & transverse generators, b) unimorph and c) bimorph

2.10. FE Model Validation

In this section the previous section load cases P and B are considered for the four harvester configurations. The harvesters are modelled using only $BaTiO_3$ and PZT-5H is ignored for validation purposes. The finite element simulations are run for the four configurations with the electric machine being a 1 ohm resistance. The orientation of each piezoelectric material varies for each configuration and related Euler angles will be presented. Note that in the bimorph series case since there are two piezoelectric material layers for the coupling matrix constant $d(3,2)$ of each layer be equal (in modulus), one layer has an orientation rotated 180 degrees around Y-axis of the other layer. For the bimorph parallel the two layers have the same material orientation. In table 6 the power results of FE model and analytical expressions are presented. As it can be seen in table 6 the relative error (RE) modulus has a maximum of 4.83% showing good agreement between FE method results and analytical expressions. The existent relative error is mainly due to a different stress distribution between the FE model and theoretical results plus boundary conditions.

Configuration	ϕ, θ, ψ (deg)	$P_{a_{FE}}$ (pw)	$P_{a_{theory}}$ (pw)	*|RE(%)|*
Long. G.	-70,50,-115	2.15e-2	2.22e-2	3.26
Trans. G.	-120,-125,5	1.45e-2	1.52e-2	4.83
Unimorph	-50,135,0	9.90e-3	1.03e-2	4.04
Bimorph Series	-55,130,-175	1.57e-2	1.54e-2	1.95
Bimorph Parallel	-110,-130,175	6.25e-2	6.04e-2	3.48

Table 6 – Piezoelectric harvesters FE method and analytical results comparison with $BaTiO_3$

The value of the electrical field and strain is also observed for the FE models in table 7 to check the validity of linear piezoelectric constitutive equations. Note that the strain is a measure of $|u_{i,K}|$ because of expression 9. As it can be seen in table 7 the strain is very low satisfying the condition $|u_{i,K}| \ll 1$. However the electrical field is not much smaller than 1 reaching order of magnitude 1×10^5 breaking the classical conditions for linear piezoelectric constitutive equations. This also shows that we are inside of section 2.7 expressions conditions since $Or[\{T\}] = 10\ MPa$ for all four configurations.

Configuration	$Max\ \|E_k\|\ (V/m)$	$Max\ \|strain\|$
Long. G.	4.01e2	8.62e-5
Trans. G.	1.03e4	9.80e-5
Unimorph	4.46e4	8.27e-5
Bimorph Series	2.52e5	1.44e-4
Bimorph Parallel	2.39e5	1.49e-4

Table 7 – Maximum electrical field and strain with $BaTiO_3$

3. Optimization & Design Variables

In this work what is desirable to optimize is the electrical machine harvested power, so this is the objective function:

$$O = P_a$$

The design variables are the Euler angles or each piezoelectric material layer orientation. The Euler angles are constrained between -180 to 180 degrees assuming only discrete values as stated in section 2.6 end.

The optimization method used is a modified simulated annealing based in the Monte Carlo step proposed in the Metropolis algorithm [31, 40]. The reason to choose a gradient free optimization method is to search relatively quick for global maximums. The algorithm is presented in annex 1. In parallel to the algorithm it

is saved the best encountered solution during the optimization. After finishing optimization the optimized and best encountered solutions are compared. It is taken the best one as the optimal. The different optimization options used in this paper are presented in table A.1 of annex 1.

4. Harvested Power Optimization Faraway Resonance

In this section it is optimized the electrical machine power using the ANSYS or FE model, varying piezoelectric material orientation for the four configurations and different loadings. The electric machine is a resistance 1 ohm. The analysis is harmonic and all loadings are 1Hz to be faraway resonance. The piezoelectric material can be $BaTiO_3$ or PZT-5H.

4.1. Loading and Boundary Conditions

The longitudinal and transverse generators are subjected to two load cases. The first load case is the load case labelled P of section 2.9. The second load case is the previous 10 MPa of load case P plus a shear stress of 40 MPa (this load is labelled PS). The shear stress is caused applying a 38 (N) force in each lateral face as illustrated in figure 5a). The boundary condition $V_2 = 0$ is applied for the load cases P and PS.
The unimorph and bimorph are subjected to two load cases. The first one is equal to load case labelled B of section 2.9 which is a tip 0.00254 (Nm) bending moment. The second load case is a tip 0.003 (Nm) torque (this load is labelled T). The torque is caused applying a 1.2 (N) force on each tip lateral faces as illustrated in figure 5b). For the two load cases the boundary conditions are zero displacements at root plus $V_2 = 0$.

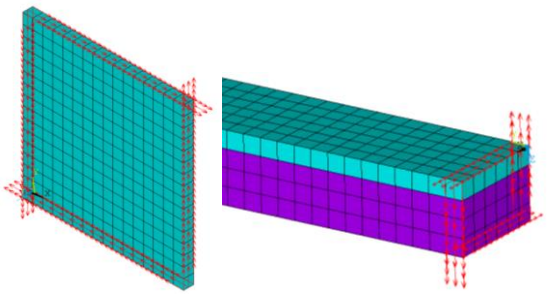

Figure 5 – Loading condition for a) longitudinal & transverse generators, b) unimorph and bimorph

4.2. Optimization Results & Discussion

The harvested power is optimized with options 1 table A.1 in annex for longitudinal and transverse generators plus unimorph and table A.1 options 2 for bimorph.

The results for longitudinal and transverse generators are presented in table 8. In this table going from left to end column it is observed the load case and configuration label, the piezoelectric material used in the configuration, the harvested power for initial orientation which is Euler angles $(0,0,0)$ orientation or classical orientation, the optimization process time, number of objective function evaluations, optimized orientation Euler angles and correspondent harvested power and finally the ratio between optimum and classical orientation powers. The optimized orientations are presented in figure 6 relative to figure 6REF) coordinate system or classical orientation. Each parallelepiped represents piezoelectric material and is aligned with Euler angles orientation or material orientation. The parallelepiped longest edge is aligned with X-axis, the smallest with Z-axis and the medium with Y-axis. The X, Y and Z axis are also represented by pink, black and red arrows respectively. The power ratio column shows that for all configurations there is an improvement in rotating $BaTiO_3$ in range 5.5 to 445.7. For the PZT-5H there is a significant improvement in rotating material only for load case PS.4. The optimization shows for PZT-5H that there are non-classic orientations which perform as good as the classical one (for example P.2). Considering now P load cases the maximum power is produced by longitudinal generator with PZT-5H $1.56 \times 10^{-1}(pw)$; for both configurations PZT-5H produces the highest power; the longitudinal generator for both piezoelectric materials produces the highest power; the ratio of maximum power between PZT-5H and $BaTiO_3$ is 7.1. In the next load cases PS, a shear is introduced and the maximum power is produced by longitudinal generator with $BaTiO_3$ $3.35 \times 10^{-1}(pw)$; for both configurations, $BaTiO_3$ produces the
highest power; the longitudinal generator continues to produce the highest power for both materials; the ratio of maximum power between $BaTiO_3$ and PZT-5H is 2.12. The orientations obtained for load cases PS are different from load cases P showing that if the loading changes, the optimum orientation can also change.

The results for unimorph and bimorph are presented in table 9. In this table the column labels mean the same as table 8 but now the Euler angles are doubled since two piezoelectric material layers are considered for bimorph (for unimorph only three). The Euler angles indexed by $1m$ refer to layer 1 or the layer delimited by potentials V_1 and V_2 in figure 2d). The other Euler angles or $2m$ refer to the other layer. In figure 7 the reference and table 9 optimized orientations are presented. It is important to note that the classical orientation for bimorph series (0,0,0,0,0,0) is the one as figure 3a) ,i.e., z-direction of one layer is opposite of the other and for bimorph parallel (0,0,0,0,0,0) corresponds to the two layers having the same orientation as shown in figure 3b). In this optimization the two bimorph piezoelectric material layers have no constraints. Now looking to the results the power ratio and optimized power values show that for all load cases there is a significant power improvement rotating $BaTiO_3$; for PZT-5H there is no significant power improvement except for T load cases. Considering now the B load cases the maximum power is generated by the bimorph parallel with PZT-5H material $6.84 \times 10^{-2}(pw)$; the bimorph parallel generates the highest power for both materials; the lowest power is generated by unimorph for both materials; the PZT-5H shows no improvement in rotation; the ratio of maximum powers between PZT-5H and $BaTiO_3$ is 1.4. In the next load cases T, the conventional orientation, can't take any power; the highest power is produced by bimorph parallel with $BaTiO_3$ $1.25 \times 10^{-2}(pw)$; the bimorph parallel continues to produce the highest power for both materials; the ratio of maximum powers between $BaTiO_3$ and PZT-5H is 16. The orientations obtained for the T load cases are different from the B load cases.

It is important to note that for the majority load cases of tables 8 and 9 the optimized orientation is not near maximums of d_{33} ,d_{32} and d_{34} showing that the optimization is not only improving these piezoelectric constants values.

The optimization time varies approximately between 1h to 13h for three or six Euler angles respectively which is acceptable.

Load Case & Configuration	*Piezo. Mat.*	P_{a_0} *(pw)*	*Time (min)*	N_{eval}	$\phi_{max}, \theta_{max}, \psi_{max}$ *(deg)*	$P_{a_{max}}$ *(pw)*	$\frac{P_{a_{max}}}{P_{a_0}}$
P.1 – Long. G.	$BaTiO_3$	3.92e-3	46.2	253	-70,50,-115 $*^1$	2.15e-2	5.5
P.2 – Long. G.	PZT-5H	1.56e-1	46.7	253	90,180,130 $*^1$	1.56e-1	1.0
P.3 – Trans. G.	$BaTiO_3$	5.05e-4	36.5	190	-120,-125,5 $*^2$	1.45e-2	28.7
P.4 – Trans. G.	PZT-5H	3.33e-2	47.4	253	-10,0,-40	3.33e-2	1.0
PS.1 – Long. G.	$BaTiO_3$	3.92e-3	47.7	253	-140,-55,-135	3.35e-1	85.4
PS.2 – Long. G.	PZT-5H	1.56e-1	48.8	253	65,20,-45	1.58e-1	1.0
PS.3– Trans. G.	$BaTiO_3$	5.05e-4	26.5	145	160,50,130	2.25e-1	445.7
PS.4 – Trans. G.	PZT-5H	3.33e-2	48.5	253	-180,40,50	5.34e-2	1.6

Table 8 – Optimization results longitudinal and transverse generators; $*^1$ orientation near a $|d_{33}|$ maximum; $*^2$ orientation near a $|d_{31}|$ maximum

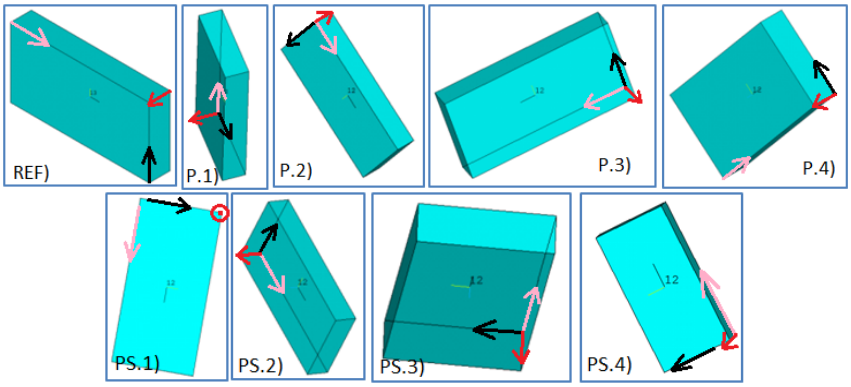

Figure 6 – Reference and optimized material orientations for P and PS load cases

Load Case & Configuration	*Piezo Mat*	P_{a_0} *(pw)*	*Time (min)*	N_{eval}	ϕ_{1m}/ϕ_{2m} ; θ_{1m}/θ_{2m} ; ψ_{1m}/ψ_{2m} *(deg)*	$P_{a_{max}}$ *(pw)*	$\frac{P_{a_{max}}}{P_{a_0}}$
B.1 – Unimorph	$BaTiO_3$	3.23e-4	56.3	253	-50; 135; 0	9.94e-3	30.7
B.2 – Unimorph	PZT-5H	1.32e-2	56.5	253	0 ; 0 ; 0	1.32e-2	1.0
B.3 – Bimorph Series C.	$BaTiO_3$	4.79e-4	783.9	813	-130/160 ; -45/-65; 5/-150	1.21e-2	25.3
B.4 – Bimorph Series C.	PZT-5H	1.71e-2	778.3	813	0/0 ; 0/0 ; 0/0	1.71e-2	1.0
B.5 – Bimorph Parallel C.	$BaTiO_3$	1.92e-3	415.4	436	0/-145 ; 55/35 ; -5/-10	4.90e-2	25.5
B.6 – Bimorph Parallel C.	PZT-5H	6.84e-2	776	813	0/0 ; 0/0 ; 0/0	6.84e-2	1.0
T.1 – Unimorph	$BaTiO_3$	0	54.4	244	-70 ; 125 ; -45 $*^3$	2.61e-3	---
T.2 – Unimorph	PZT-5H	0	57.2	253	-40 ; 55; 45	1.77e-4	---
T.3 – Bimorph Series C.	$BaTiO_3$	0	817.8	813	-140/155 ; -120/-135 ; 130/35	3.38e-3	---
T.4 – Bimorph Series C.	PZT-5H	0	783.1	813	165/105 ; -55/-60 ; -130/-50	2.51e-4	---
T.5 – Bimorph Parallel C.	$BaTiO_3$	0	791.3	813	-80/100 ; 50/130 ; 55/120	1.25e-2	---
T.6 – Bimorph Parallel C.	PZT-5H	0	772.4	813	85/30 ; 115/75 ; -130/120	7.83e-4	---

Table 9 – Optimization results unimorph and bimorph; $*^3$ orientation near a $|d_{34}|$ maximum

ZZZ

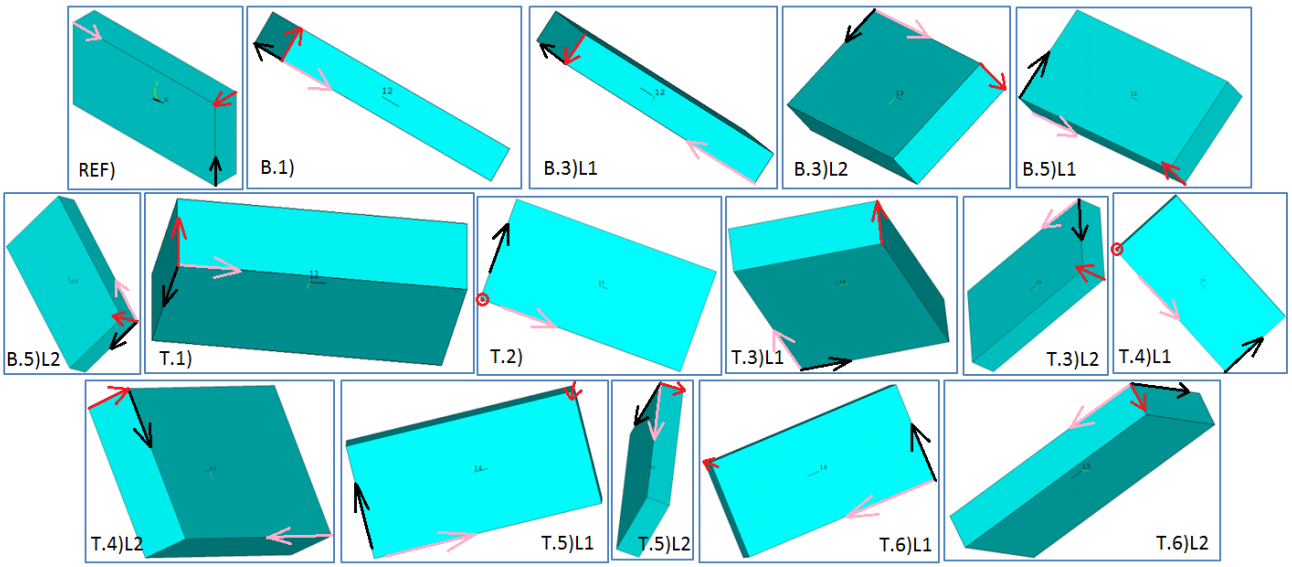

Figure 7 – Reference and optimized materials orientations for B and T load cases

5. Harvested Power Optimization in Resonance

In this section the previous unimorph and bimorph harvesters are changed so that its first resonant frequency without damping and electric machine is lower or near 140 (Hz) which is inside the range of ambient vibrations 1 to 200 (Hz) [7]. Next the materials damping is considered and it is shown its effect faraway and in resonance. The harvested power is optimized for a near resonance frequency considering B load cases. After that the power sensibility to resistance value is investigated for maximum power orientations. In the final section the power is optimized for a set of frequencies.

5.1. Added Mass and Harvesters Tuning

There are various methods to tune a unimorph and bimorph harvesters frequency. In this paper one of the methods used is to add a tip mass. This tip mass is made of Tantalum, a high density and high corrosion resistant material. Its properties are presented in table 10 [41]. The tip mass is added to the harvesters as presented in figure 8 ,i.e. , adding mass to the cantilever tip with length $L_{tip.mass}$, constant cross section width W of table 5 and the same thickness of substrate plus piezoelectric material layers. Two other options are also used to tune harvesters. One consists of increasing the beam length by increasing piezoelectric material layers length and substrate length L_{piezo}. The other one is to decrease substrate thickness S_{thick}. After doing a modal analysis parametric study (varying $L_{tip.mass}$, L_{piezo}, S_{thick}) using $BaTiO_3$ with (0,0,0) orientation or

Tantalum	*Value*
Density (Kg/m^3)	16400
Young Modulus (GPa)	186.2
Poisson Ratio	0.34

Table 10 – Tantalum material properties

classical in unimorph and bimorph, it is decided to use in both configurations $L_{piezo} = 5\ (cm)$, $L_{tip.mass} = 0.5\ (cm)$, $S_{thick} = 0.05\ (cm)$. This corresponds to have a 1st modal or bending frequency of 135.2 and 143.5 (Hz) for unimorph and bimorph respectively. The tuned unimorph is named UniT and the tuned bimorph BimpT.

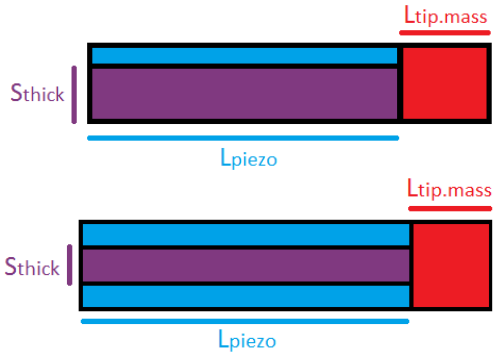

Figure 8 – Harvesters frequency tuning variables a) unimorph, b) bimorph; blue – piezoelectric material, red – tantalum, rocky - brass

5.2. Material Hysteretic Damping & Its Influence in Harvested Power

The materials used in the harvesters have hysteretic damping which may reduce the vibrations amplitude significantly and the harvested power consequently. The hysteretic damping is measured by the quality factor Q which is related to the damping ratio ζ by expression 18. This damping ratio is the ratio between present damping c and critical damping c_c. The

$$\zeta = \frac{1}{2Q} = \frac{c}{c_c} \quad (18)$$

harvesters materials mechanical quality factor is presented in table 11. These values are obtained from [42], [43] and [19]. The tantalum hysteretic damping is ignored in this work. Note in table 11 the material with maximum damping is the PZT-5H.

Material	*Q*
Brass	1000
$BaTiO_3$	1300
PZT-5H	32

Table 11 – Harvesters materials quality factor

In this section the objective is to analyze the influence of mechanical quality factor near and far resonance for a tuned configuration. To do this it is observed the different configurations power with and without damping, varying the

frequency. Here it is presented the unimorph cantilever power with PZT-5H (0,0,0) since this material has the highest damping (or the lowest quality factor) as an example of what happens. The considerate loading and boundary conditions are the same as load case B of section 4.1. This means that the tip bending moment is applied in tantalum tip. It is also used a 1 (ohm) resistance as before. The hysteretic damping is inserted into ANSYS as an equivalent viscous damping by specifying the damping ratio for each material which is assumed to be constant. The results are presented in table 12 far resonance and in figure 9 near resonance with a frequency step size of 0.4 Hz. As it can be seen in table 12, the relative difference percentage (RD%) is very small showing that the damping is not necessary to be considered faraway resonance. The results presented in figure 9 show that it is necessary to consider

$f_1(Hz)$	Q	*Power* (pw)	*RD%*
1	No	5.146e-1	0.04
1	Yes	5.148e-1	

Table 12 – Tuned unimorph Q power influence

material hysteretic damping near resonance. Note in this figure that the peak frequency 107.4 Hz is also the same for both models.

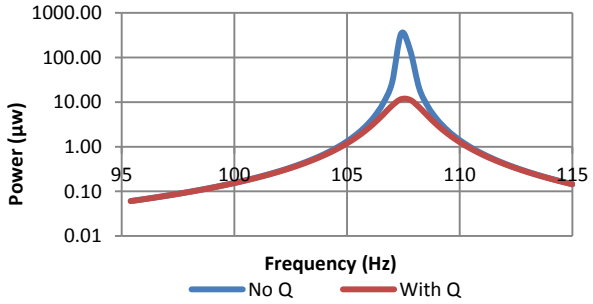

Figure 9 – Tuned unimorph power results near resonance with damping and without

5.3. Power Optimization Results & Discussion

The resistance 1 (ohm) electrical power is optimized near resonance. This is done starting with piezoelectric material optimized orientations of table 9. The objective is to know if the previous optimal orientations continue to be optimums near resonance. The loading & boundary conditions are the same (note tip moment is applied in tantalum) as section 4.1. It is needed to identify an excitation frequency very near resonance peak. This is done running a modal analysis for table 9 bending optimized orientations without electrical circuit and material damping. The excitation frequency will be the first modal frequency. The various frequencies for the different configurations are presented in table 13. Next the harvested power is optimized for the referred frequencies. It is used optimization options 1 of annex A.1 for unimorph and options 2 for bimorph. The numerical results are presented in table 14. Each column means the same as table 9. The respective optimized orientations are presented in figure 10. As it can be seen in table 14 and figure 10 there is significant power improvement for all load cases in rotating the piezoelectric materials. The maximum power is produced by $BaTiO_3$ bimorph parallel $1.92\ (mw)$. For all configurations $BaTiO_3$ produces three orders of magnitude more power than PZT-5H because it has a significantly higher mechanical quality factor, i.e., less damping. The maximum power for both materials continues to be produced by bimorph parallel configuration as in faraway resonance. The configuration that produces less power for both materials is the bimorph series; this is different faraway resonance where the unimorph configuration produced the lowest power for both materials. Relatively to faraway resonance, the power produced near resonance has increased 1×10^{11} orders of magnitudes for $BaTiO_3$ and 1×10^{8} order of magnitudes for PZT-5H. This super increase is mainly due to be near resonance. Looking now to the orientations of figure 10 it is noted these ones are different of figure 7 orientations for B load cases. This means that the optimal orientation faraway resonance is different from the one optimal near it.

Load Case & Configuration	*Piezo Mat*	$\phi_{1m}/\phi_{2m}\ ;\theta_{1m}/\theta_{2m}\ ;\ \psi_{1m}/\psi_{2m}$ *(deg)*	$f_1(Hz)$
B.7 – UniT	$BaTiO_3$	-50; 135; 0	142.3
B.8 – UniT	PZT-5H	0 ; 0 ; 0	110.5
B.9 – BimpT Series C.	$BaTiO_3$	-130/160 ; -45/-65; 5/-150	148.9
B.10 – BimpT Series C.	PZT-5H	0/0 ; 0/0 ; 0/0	107.2
B.11 – BimpT Parallel C.	$BaTiO_3$	0/-145 ; 55/35 ; -5/-10	151.7
B.12 – BimpT Parallel C.	PZT-5H	0/0 ; 0/0 ; 0/0	107.2

Table 13 – Harvesters 1st modal frequencies

Load Case & Configuration	*Piezo Mat*	P_{a_0} *(µw)*	*Time (min)*	N_{eval}	$\phi_{1m}/\phi_{2m}\ ;\theta_{1m}/\theta_{2m}\ ;\ \psi_{1m}/\psi_{2m}$ *(deg)*	$P_{a_{max}}$ *(µw)*	$\frac{P_{a_{max}}}{P_{a_0}}$
B.7 – UniT	$BaTiO_3$	0.53	76.1	199	175 ; -145 ; -160	1916.90	3616.8
B.8 – UniT	PZT-5H	0.90	100.2	253	5 ; 150 ; -180	1.92	2.1
B.9 – BimpT Series C.	$BaTiO_3$	0.50	2449.2	610	70/-170 ; 30/-40 ; -55/-170	1052.35	2104.7
B.10 – BimpT Series C.	PZT-5H	0.60	3362.2	813	-65/140 ; -35/30 ; 155/175	1.23	2.1
B.11 – BimpT Parallel C.	$BaTiO_3$	0.98	2241.5	552	-65/-85 ; 30/50 ; -175/-75	8062.17	8227.3
B.12 – BimpT Parallel C.	PZT-5H	2.36	3495.6	813	-60/125 ; 30/30 ; 5/0	5.08	2.2

Table 14 – Tuned harvesters power optimization

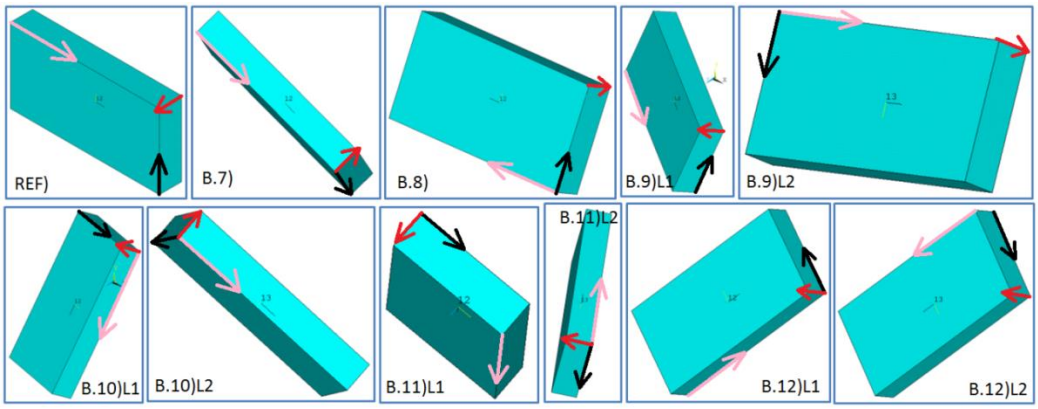

Figure 10 – Reference and optimized materials orientations for B load cases near resonance

Looking to the orientations in table 14 it is important to note these ones are not near maximums of d_{33}, d_{32} or d_{34} showing that the optimization is not only improving these piezoelectric constants values.

The optimization takes much more time than table 9 for the bending load cases. This is due to the significant increase of elements number due to frequency tuning. The optimization time varies between 1.3 hours and 58 hours which is acceptable.

The power has been optimized for the 1st modal frequency of the different configurations. The frequency versus power is shown in figures 11 to 12 for the optimal orientations and classic orientations. It is presented as triangles the optimum obtained powers. As it can be seen in figure 11, the optimized power for $BaTiO_3$ is the power peak and the classical orientation power peak is significantly lower than the optimized one. For the PZT-5H the optimized power is not the peak plus classical orientation peak is higher than the optimal one. As it can be seen in figures 11 and 12 the peak power produced by $BaTiO_3$ is around at least 3 orders of magnitude higher than PZT-5H. It is observed a general increase in power near resonance as expected since observed in other works [19].

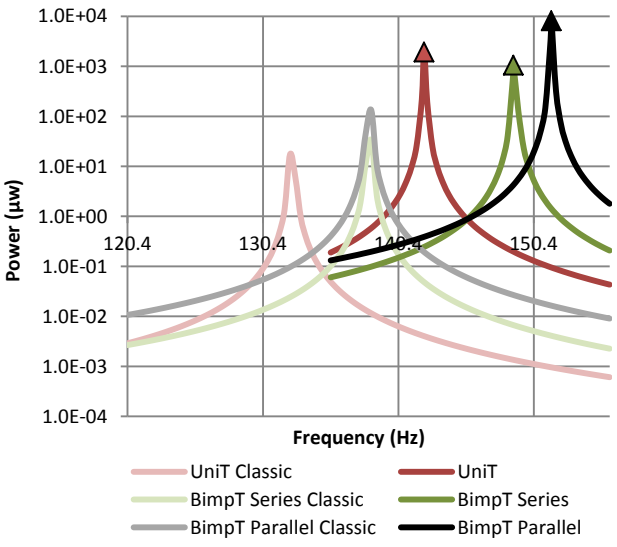

Figure 11 – Power vs frequency $BaTiO_3$

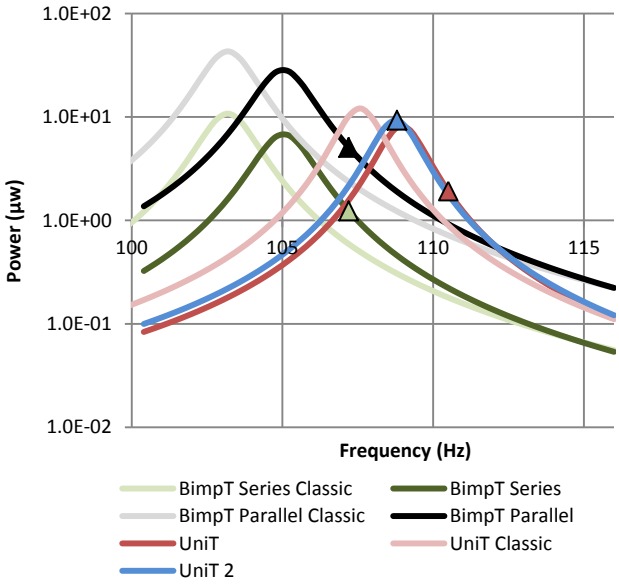

Figure 12 – Power vs frequency PZT-5H

The optimized power for PZT-5H is not the power peak. To cause power peak optimization and to know if the current peak power can be increased it is decided to do an additional power optimization (UniT 2) for the PZT-5H configurations but now the excitation frequency will be figure 12 peaks frequencies. For the bimorph series and parallel no improvement is verified but for unimorph it is found a peak power improvement of 1.2 being 9.31 (μw). The power vs frequency for this optimized solution is presented in figure 12 as blue (UniT 2). The new obtained optimized orientation is (110,25,0) degrees. This orientation is presented in figure 13. As it can be seen this orientation is very different from previous one (figure 10 B.8).

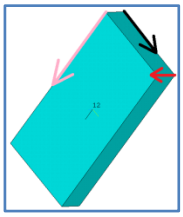

Figure 13 – Optimized material orientation B.8) second optimization

5.4. Harvested Power Sensitivity to Resistance

In this section it is studied the power sensibility to resistance. To do this the UniT, BimpT Series and BimpT Parallel configurations of section 5.3 with maximum power orientations are run for different resistances and respective power peak frequency. The power vs resistance curves are presented in figures 14 and 15 for $BaTiO_3$ and PZT-5H respectively. In table 15 it is presented the excitation frequency, optimum resistance and power for the different configurations. As it can be seen in figures 14 and 15 plus table 15 there is an optimum resistance value as expected according to [3]. This value changes with material and configuration; the "difference" between power generated by PZT-5H and $BaTiO_3$ is of an order of magnitude 10 which is much lower than the one observed in table 14 (three orders of magnitude). For all configurations the maximum power is generated by configurations with BaTio3 and the maximum power continues to be produced by bimorph parallel for both materials. For PZT-5H bimorph series and parallel with optimum resistance value the produced power is near the same. This was also observed in [19] for the same material and orientation. For $BaTiO_3$ the same effect is not observed, showing that it cannot happen if the material is changed.

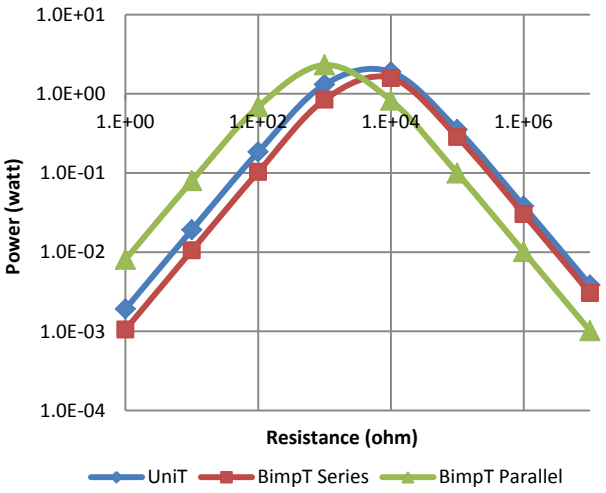

Figure 14 – Power vs resistance for $BaTiO_3$ configurations

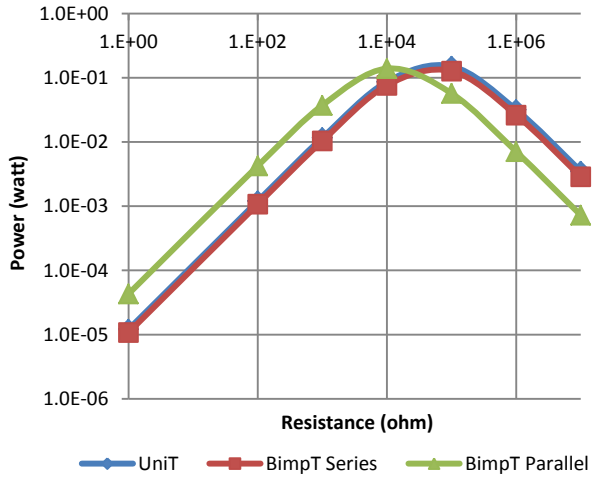

Figure 15 – Power vs resistance for PZT-5H configurations

Configuration	*Material*	$f_{exc}(Hz)$	*Ropt (ohm)*	*Power (watt)*
UniT	BaTio3	142.3	1.0E+04	1.89
UniT	PZT-5H	107.6	1.0E+05	0.15
BimpT Series	BaTio3	148.9	1.0E+04	1.58
BimpT Series	PZT-5H	103.2	1.0E+05	0.13
BimpT Parallel	BaTio3	151.7	1.0E+03	2.31
BimpT Parallel	PZT-5H	103.2	1.0E+04	0.14

Table 15 – Peak power for optimum resistance

5.5. UniT Power Optimization for Various Frequencies, Results & Discussion

In this section it is optimized the UniT power for a set of discrete frequencies. The objective function value is changed to a discrete sum of powers (for different frequencies) given by expression 19 where N is an integer. The design variables continue to be the piezoelectric materials orientations. Looking

$$O = \sum_{i=1}^{N} P_{a_i} \quad (19)$$

to figures 11 and 12 it is decided to use frequencies in the range 130 to 150 (Hz) and 95 to 115 (Hz) for $BaTiO_3$ and PZT-5H respectively. The frequency step used is 1 Hz meaning that $N = 21$ for both materials. The optimization options are options 1 of annex 1. The initial orientations are (175,-145,-160) or table 14 orientation for $BaTiO_3$ and (0,0,0) or classical for PZT-5H (these are orientations for maximum peak power). The power results are presented in table 16 and figure 16 (squares are interpolation points). In this table O_0 is the initial objective function value and O_{max} the optimized one. The $BaTiO_3$ shows a significant power improvement. The power peaks ratio for $BaTiO_3$ is 1.7. It is important to note that the term contributing more for the objective function value in the $BaTiO_3$ case is the power peak. PZT-5H classical orientation is not beat showing this orientation as one already optimized for various frequencies. The new $BaTiO_3$ orientation is presented in figure

Material	$O_0\ (\mu w)$	*Time*	N_{eval}	$\phi, \theta, \psi\ (deg)$	$O_{max}(\mu w)$
$BaTiO_3$	115.2	615.4	172	-40, -55, -175	3026.3
PZT-5H	29.9	989.2	253	0, 0, 0	29.9

Table 16 – UniT various frequencies optimization

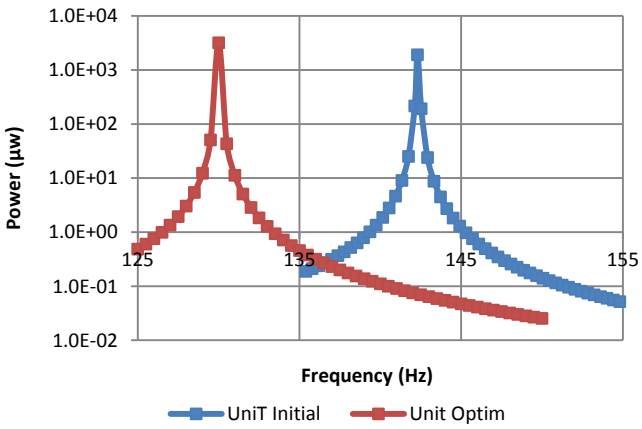

Figure 16 – UniT power vs frequency with $BaTiO_3$

17. Note this orientation is different from the previous B.7) and B.1) orientations.

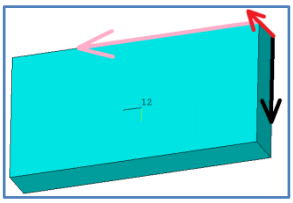

Figure 17 – UniT with $BaTiO_3$ optimized orientation

6. Conclusions & Future Work

In section 2 very high electrical fields are observed for piezoelectric harvesters creating the need to study in more depth the applicability of linear piezoelectric constitutive equations in the presence of high electrical fields. Simple expressions are presented to design piezoelectric vibrations energy harvesters with specific loadings faraway resonance.

In section 4 it is shown faraway resonance that the best material for an energy harvester configuration can change with the loading conditions; the best material orientation can change with harvester configuration and loading conditions (for a specific harvester).

In section 5 the need to include hysteretic damping near resonance is shown after tuning unimorph and bimorph configurations for ambient vibrations. The power optimization for the first modal frequency shows $BaTiO_3$ as a material capable of producing more power than PZT-5H, i. e., around three orders of magnitude higher. In resonance the optimized harvester material orientations can be different of the ones faraway resonance. The power sensibility to resistance shows that for optimum resistance value the $BaTiO_3$ harvesters produces one order of magnitude more power than PZT-5H harvesters. The various frequencies power optimization near resonance shows PZT-5H has a material already optimized for various frequencies and that $BaTiO_3$ optimal orientation changes.

The obtained results encourage piezoelectric material tailoring to increase harvested power faraway resonance and in resonance. The tailoring method can involve building piezocomposites with various materials & different orientations and so on. The simple expressions obtained faraway resonance can be used as a starting point. The obtained results in resonance show that the material orientation is not rotating to orientations of maximum piezoelectric constants d_{33}, d_{32} and d_{34}. Near resonance harvested power simple expressions cannot be obtained. The finite element method provides a suitable tool to simulate the harvesters and calculate power.

References

[1] H. A. Sodano, D. J. Inman & G. Park. *A review of power harvesting from vibration using piezoelectric materials*. Shock and Vibration Digest, volume 36, pages 197-206. 2004

[2] S. R. Anton & H. A. Sodano. *A review of power harvesting using piezoelectric materials (2003-2006)*. Smart Materials and Structures, volume 16, number 3. 2007

[3] L. Zhang. *Analytical Modelling and Design Optimization of Piezoelectric Bimorph Energy Harvester*. PhD Thesis, The University of Alabama, USA. 2010

[4] L. Zhang, K. A. Williams & Z. Xie. Evaluation of Analytical and Finite Element Modeling on Piezoelectric Cantilever Bimorph Energy Harvester. Transactions of the Canadian Society for Mechanical Engineering, Volume 37, Number 3. 2013

[5] L. Zhang, K. A. Williams & Z. Xie. Development and Validation of an Enhanced Coupled/Field Model for PZT Cantilever Bimorph Energy Harvester. Mathematical Problems in Engineering, Volume 2013, ID 980161. 2013

[6] J. Yang, H. Zhou, Y. Hu & Q. Jiang. *Performance of a Piezoelectric Harvester in Thickness-Stretch Mode of a Plate*. IEEE Transactions on Ultrasonics Ferroelectrics and Frequency Control, Volume 52, pages 1872-1876. 2005

[7] S. Roundy, P. K. Wright & J. Rabaey. *A study of low level vibrations as a power source for wireless sensor nodes*. Computer Communications, volume 26, pages 1131-1144. 2003

[8] D. Berlincourt & H.H. A. Krueger. *Properties of Piezoelectricity Ceramics*. Technical Publication TP-226, Morgan Electro Ceramics. 2014

[9] T. Eggborn. *Analytical Models to Predict Power harvesting with Piezoelectric Materials*. MSc Thesis, Virginia Polytechnic Institute and State University, USA. 2003

[10] H. A. Sodano, D. J. Inman & G. Park. *Estimation of Electric Charge output for Piezoelectric Energy Harvesting*. Strain Journal, volume 40, pages 49-58. 2004

[11] A. Erturk, D. J. Inman. *On Mechanical Modeling of Cantilevered Piezoelectric Vibration Energy Harvesters*. Journal of Intelligent Material Systems and Structures, volume 19, pages 1311-1325. 2008

[12] R. Dunsch, J. Breguet. *Unified mechanical approach to piezoelectric bender modelling*. Sensors and Actuators A: Physical, volume 134, pages 436-446. 2007

[13] J. M. Dietl, A. M. Wickenheiser & E. Garcia. *A Timoshenko beam model for cantilevered piezoelectric energy harvesters*. Smart Materials and Structures, volume 19, number 5.2010

[14] C. Huang, Y. Y. Lin & T. A. Tang. *Study on the tip-deflection of a piezoelectric bimorph cantilever in the static state*. Journal of Micromechanics and Microengineering, volume 14, number 4. 2004

[15] J. Ajitsaria, S. Y. Choe & D. J. Kim. *Modeling and analysis of a bimorph piezoelectric cantilever beam for voltage generation*. Smart Materials and Structures, volume 16, number 2. 2007

[16] A. Erturk & D. J. Inman. *A Distributed Parameter Electromechanical Model for Cantilevered Piezoelectric Energy Harvesters*. Journal of Vibration and Acoustics, volume 130, issue 4. 2008

[17] N. E. duToit, B. L. Wardle & S. Kim. *Design Considerations for MEMS-Scale Piezoelectric Mechanical Vibration Energy Harvesters*. Integrated Ferroelectrics, volume 71, pages 121-160. 2005

[18] S. Avdiaj, J. Setina & N. Syla. *Modeling of the Piezoelectric Effect Using the Finite-Element Method (FEM)*. Materials and Technology, volume 43, pages 283-291. 2009

[19] M. Zhu, E. Worthington & J. Njuguna. *Analyses of Power Output of Piezoelectric Energy-Harvesting Devices Directly Connected to a Load Resistor Using a Coupled Piezoelectric-Circuit Finite Element Method*. IEEE Transactions on Ultrasonics Ferroelectrics and Frequency Control, volume 56, pages 1309-1318. 2009

[20] C. Bendigeri, R. Tomar, S. Basavaraju & K. Arasukumar. *Detailed Formulation and Programming Method for Piezoelectric Finite Element.* International Journal of Pure and Applied Sciences and Technology, volume 7, pages 1-21. 2011

[21] V. Piefort. *Finite Element Modelling of Piezoelectric Active Structures*. PhD Thesis, Université Libre de Bruxelles, Belgium. 2001

[22] A. Kumar, A. Sharma, R. Kumar, R. Vaish & V. S. Chauhan. *Finite element analysis of vibration energy harvesting using lead-free piezoelectric materials: A comparative study*. Journal of Asian Ceramic Societies, volume 2, pages 138-143. 2014
[23] C. M. Junior, A. Erturk, D. J. Inman. *An electromechanical finite element model for piezoelectric energy harvester plates*. Journal of Sound and Vibration, volume 327, pages 9-25. 2009
[24] J. B. Min, K. P. Duffy, B. B. Choi, A. J. Provenza & N. Kray. *Piezoelectric Vibration Damping Study for Rotating Composite Fan Blades*. NASA/TM-2012-217648, USA. 2012
[25] A. J. Masys, W. Ren, G. Yang & B. K. Mukherjee. Piezoelectric strain in lead zirconate titante ceramics as a function of electrical field, frequency, and dc bias. Journal of Applied Physics, volume 94, pages 1155-1162. 2003
[26] A. M. Rajapurkar. *Loss Mechanisms in Piezoelectric PZT Ceramics and Single Crystals*. MSc Thesis, The Pennsylvania State University, USA. 2008
[27] E. C. N. Silva, J. S. O. Fonseca & N. Kikuchi. *Optimal design of periodic piezocomposites*. Computer Methods in Applied Mechanics and Engineering, volume 159, pages 49-77. 1998
[28] E. C. N. Silva, S. Nishiwaki, J. S. O. Fonseca, N. Kikuchi. *Optimization methods applied to material and flextensional actuator design using the homogenization method*. Computer Methods in Applied Mechanics and Engineering, volume 172, pages 241-271. 1999
[29] J. M. Guedes & N. Kikuchi. *Preprocessing and Postprocessing for Materials Based on the Homogenization method with Adaptive Finite Element Methods*. Computer Methods in Applied Mechanics and Engineering, volume 83, pages 143-198. 1990
[30] K. P. Jayachandran, J. M. Guedes & H. C. Rodrigues. *Homogenized electromechanical properties of crystalline and ceramic relaxor ferroeletric 0.58Pb($Mg_{1/3}Nb_{2/3}$)O_3-0.42PbTiO_3*. Smart Materials and Structures, volume 16, pages 1534-1541. 2007
[31] K. P. Jayachandran, J. M. Guedes & H. C. Rodrigues. *Optimal configuration of microstructure in ferroelectric materials by stochastic optimization*. Journal of Applied Physics, volume 108, issue 2. 2010
[32] J. Yang. *An Introduction to The Theory of Piezoelectricity*. Springer. 2005
[33] Internet Website PIEZO SYSTEMS INC, http://www.piezo.com/tech2intropiezotrans.html. 03/11/2014
[34] M. Zgonik et al. *Dielectric, elastic, piezoelectric, electro-optic, and elasto-optic tensors for $BaTiO_3$ crystals*. Physics Review B, volume 50, pages 5941-5950. 1994
[35] Internet Website Efunda, Materials Data, Piezo Materials. http://www.efunda.com/materials/piezo/material_data/matdata_output.cfm?Material_ID=PZT-5H . 04/11/2014
[36] Internet Website E-ZLOK, Technical Info, Free-Cutting Brass. http://www.ezlok.com/TechnicalInfo/MPBrass.html . 04/11/2014
[37] Internet Website The Engineering ToolBox, Resistivity. http://www.engineeringtoolbox.com/resistivity-conductivity-d_418.html . 04/11/2014
[38] H. Goldstein. *Classical Mechanics*. Addison-Wesley. 1978
[39] F. P. Beer et al. *Mechanics of Materials, 6^{th} edition*. McGrawHill. 2012
[40] J. S. Arora. *Introduction to Optimum Design*. Elsevier Academic Press. 2004
[41] Internet Website Efunda, Materials Data, Elements. http://www.efunda.com/materials/elements/element_info.cfm?Element_ID=Ta . 07/11/2014
[42] K. Nakamura, K. Kakihara, M. Kawakami & S. Ueha. *Measuring vibration characteristics at large amplitude region of materials for high power ultrasonic vibration system*. Ultrasonics, volume 38, pages 122-126. 2000
[43] Internet Website APC International, Properties of BaTio3 https://www.americanpiezo.com/product-service/bati03.html. 12/11/2014

Annex 1 – Simulated Annealing Script & Options

The simulated annealing algorithm used in this paper is presented in Script 1.

----------*Script 1*----------

STEP1. Define $\mathrm{Mn_r}$ maximum number of consecutive rejections; $\mathrm{Mn_t}$ maximum number of tries within one temperature; $\mathrm{Mn_S}$ maximum number of successes within one temperature; K_B a numerical constant; $\mathrm{T_i}$ Initial temperature; $\mathrm{T_{STOP}}$ stop temperature; $\overline{DV}_0$ initial design variables vector; r cooling factor. Start counters number of tries $\mathrm{N_t} = 0$; number of successes $\mathrm{N_S} = 0$; number of consecutive rejections $\mathrm{N_r} = 0$. Start temperature $T_L = T_\mathrm{i}$ with counter $L = 0$. Start number of function evaluations counter $k = 0$. Start optimum design variables as $\overline{DV}_{\mathrm{optim}} = \overline{DV}_0$ and calculate respective objective function $O_k = O_{\mathrm{optim}}$.

STEP2. $\mathrm{N_t} = \mathrm{N_t} + 1$;

STEP3. If $\mathrm{N_t} \geq \mathrm{Mn_t}$ or $\mathrm{N_S} \geq \mathrm{Mn_S}$ go to STEP4. Else go to STEP6.

STEP4. If $T_L < \mathrm{T_{STOP}}$ *or* $\mathrm{N_r} \geq \mathrm{Mn_r}$ END. Else go to STEP5.

STEP5. Cool the temperature: $L = L + 1$ and $T_L = T_{L-1} r$; $\mathrm{N_t} = 1$; $\mathrm{N_S} = 1$; $k = k + 1$;

STEP6. Do $k = k + 1$. Generate new design variables $\overline{DV}_k$ and a corresponded objective function value O_k

STEP7. If $O_k > O_{\mathrm{optim}}$ $\overline{DV}_{\mathrm{optim}} = \overline{DV}_k$ *and* $O_{\mathrm{optim}} = O_k$, do $\mathrm{N_S} = \mathrm{N_S} + 1$, $\mathrm{N_r} = 0$ and go to STEP2.

STEP8. Generate a random number r_d between 0 and 1; If $r_d < \mathrm{e}^{(O_k - O_{k-1})/(K_B T_L)}$ do $\overline{DV}_{\mathrm{optim}} = \overline{DV}_k$, $O_{\mathrm{optim}} = O_k$ and $\mathrm{N_S} = \mathrm{N_S} + 1$. Else do $\mathrm{N_r} = \mathrm{N_r} + 1$. Go to STEP2.

The different optimization options used in this paper are presented in table A.1.

Optimization Algorithm	Value – Options 1	Value – Options 2
$\mathbf{Mn_r}$	100	400
$\mathbf{Mn_t}$	10	30
$\mathbf{Mn_S}$	100	100
$\boldsymbol{K_B}$	1	1
$\mathbf{T_i}$	100	100
$\mathbf{T_{STOP}}$	0.3	0.3
$\boldsymbol{r}$	0.8	0.8

Table A.1 – Optimization options